Computer Assisted Mechanics and Engineering Sciences, 6: 115–130, 1999.

A reactedness model for local extinction and reignition phenomena in turbulent jet diffusion flames

Panayiotis Koutmos and Costas Mavridis
Department of Mechanical Engineering
University of Patras
Patras, Rio 26500 Greece

(Received June 4, 1998)

An approach for modeling finite-rate chemistry effects such as local extinction and reignition in piloted diffusion flames of $CO/H_2/N_2$ or CH_4 and air is presented. A partial equilibrium/two-scalar exponential PDF combustion model is combined with a 2D Large Eddy Simulation procedure employing an anisotropic subgrid eddy-viscosity and two equations for the subgrid scale turbulent kinetic and scalar energies. Statistical independence of the PDF scalars is avoided and the required moments are obtained from an extended scale-similarity assumption. Extinction is accounted for by comparing the local Damkohler number against a 'critical' local limit related to the Gibson scalar scale and the reaction zone thickness. The post-extinction regime is modelled via a Lagrangian transport equation for a reactedness progress variable that follows a linear deterministic relaxation to its mean value (IEM). Comparisons between simulations and measurements suggested the ability of the method to calculate adequately the partial extinction and reignition phenomena observed in the experiments.

Key words: $CO/H_2/N_2$ or CH_4 flames, extinction and reignition, partial equilibrium model, Large Eddy Simulations, Lagrangian models.

Notations

B	reactedness progress variable
C_{kij}	SGS model constants
Da	Damkohler number
D_j	central fuel-jet diameter
f/f^*	mixture fraction/normalized
$f_{\text{L,R}}$	Lean/Rich mixture fraction flammability limits
IEM	Interaction by Exchange with the Mean model
J	Jacobian of transformation (2-S PDF)
k_{f}	forward reaction rate constant
k_{e}	equilibrium constant
k_s, k_{fs}	energy/fluctuation energy
k_r, k_{fr}	resolved energy/fluctuation energy
L_t	turbulence length scale
M_i	molecular weight of specie i
u, v	axial and transverse velocities
u_e, u_p, u_j	coflow air, pilot burnt gas and fuel jet velocity
P, PDF	Probability Density Function
P_F	cumulative propability of ignition
Re_t	local turbulent Reynolds number
R_u	universal gas constant
R	resolved fluctuations
R_A	Annular air radius

R_p	Annular burnt gases radius
R_j	Central fuel jet radius
$\dot{r}_{CO_2}$	reaction rate of CO_2
Sc	Schmidt number
S_B	source term
S_{ij}	resolvable strain tensor
T	temperature
x_i	coordinate directions ($i = 1, 2$)
Y_i	mass concentration
$Y^*_{CO_2}$	normalized concentration of CO_2
$\mathbf{Y}_E$	undisturbed burning state vector
$\mathbf{Y}_I$	inert mixing state vector
$\mathbf{Y}_Q$	transition gas state vector

Greek symbols

δ_{ij}	Kronecker delta ($\delta_{ij} = 0$ for $i \neq j$, $\delta_{ij} = 1$ for $i = j$)
Δf_R	reaction zone width in f space
$\Delta, \Delta x, \Delta y$	characteristic mesh sizes
ε_f	dissipation rate of the scalar fluctuations
υ_t	eddy-viscosity coefficient
ρ	density
Σ_f	scalar scale
σ_k	turbulent Prandtl number
τ_k	Kolmogorov time scale
τ_{ch}	chemical time scal
τ_{ij}, σ_{ij}	stresses
$\tau_t, \tau_\lambda, \tau_e$	time-scales of turbulence
τ_{id}	turbulence/chemical ignition delay time

Operators

$\ldots'$	turbulent (subgrid-scale) quantity
$<\widetilde{\ldots}>$	Favre resolved quantities
$<\overline{\ldots}>$	time-averaged value

Subscripts

A, a	air
ch	chemical
cr	critical
f	fuel
i	i = 1, 2 cartesian coordinates
i, j	tensor notation
L	Lean
R	Rich
s	subgrid scale, stoichiometric
t	turbulent flow

Superscripts

*	normalized value

1. INTRODUCTION

The prediction of reacting flows with strong turbulence/chemistry interactions leading to localized extinction and reignition phenomena poses a significant challenge in the effort to develop efficient computational models for combustors. Under strong deviations from the fast chemistry assumption the adequate description of the local flame structure requires the introduction of a large number of reactive scalars in the basic conserved scalar approach [1, 2]. Multi-scalar approaches can sometimes be avoided if the local gas state is parameterized in terms of a local Damkohler number and appropriate extinction criteria are employed [3, 4]. The usefulness of such methods depends on how adequately these represent the flame structure close to extinction [5] and confidence in their application warrants further investigations into their development. Recent detailed non-intrusive space and time-resolved measurements of the local flame structure [6, 7, 8, 9] have allowed insight into the extinction/reignition and monomodal/bimodal behavior in flames with significant finite-rate chemical kinetic effects. Their findings have helped to develop and extend available combustion models [1, 3, 4, 10, 11] to include finite-rate chemistry effects in current modeling techniques. A related and equally significant issue in turbulent flame modeling technology is the influence of large scale vortical structures and flow unsteadiness on entrainment, heat release and stability characteristics of turbulent flames [12, 13]. As these dynamic interactions may be actively enhanced by transient extinction/reignition phenomena and *vice versa* [14] their effects merit inclusion in suitable modeling approaches.

This investigation then attempts to address the above issues and develop a modeling tool for studying turbulent flames with finite-rate kinetic effects while avoiding the complexity of multi-scalar treatments. Such a procedure should be readily extentable to bluff-body flames as they are also of direct relevance to combustor design. The 2D Large Eddy Simulation procedure of [13] is here employed together with a constrained partial equilibrium/two-scalar exponential PDF (Propability Density Function) model that treats turbulence/chemistry interactions at the Sub-Grid Scale (SGS) level. Statistical independence of the PDF variables is avoided in the light of recent experimental work ([17]); the SGS moments required to close the PDF are evaluated assuming scale-similarity between resolved and unresolved scalar fluctuations. Extinction is modeled by comparing the local Damkohler number against its 'critical' local value. Transient post-extinction effects and reignition are modeled via a Lagrangian transport equation for a reactedness progress variable exploiting a linear deterministic relaxation of the mixing quantity to its mean value ([16]). Computations are compared with the measurements of [8, 9] for piloted $CO/H_2/N_2$ diffusion flames exhibiting significant degrees of localized extinction and reignition. Emphasis is placed here in the adequate description of the local flame extinction behavior. Experimental observations [5, 8, 9] suggest that $CO/H_2/N_2$ flames proceed gradually to global blow-off without exhibiting localized extinction while methane [6, 7] and other hydrocarbon flames display a bimodal approach to global extinction in rich mixtures and a monomodal product composition for richer mixtures. Reference therefore to sample calculations for CH_4 flames [6, 7] is also made to establish the present model's capability to follow the experimental trend and reproduce several important features of these complex flames.

2. FLAME CONFIGURATION STUDIED

The experimental set up of [6, 8] is used in the computations (Fig. 1). The piloted burner consists of a central fuel jet ($45\%CO/15\%H_2/40\%N_2$ or CH_4) 7.2 mm in diameter surrounded by a stoichiometric, lit, premixed pilot flame (of either $45\%CO/15\%H_2/40\%N_2$ or CH_4 and air depending on the main fuel tested) 18 mm in diameter and an outer annular air supply of 320 mm in diammeter. The coflow air velocity, u_e, is maintained at 15 m/s. The pilot unburnt gas velocity, u_p, is 4 and 1m/s for the two fuels used. [6, 7, 8, 9] have reported measurements for a range of flames obtained by varying the fuel bulk velocity. The following flames were investigated, flames B and C, with central fuel velocities of 41 and 48 m/s respectively for CH4 and flames A1, B1, C1, D1 and E1 with fuel

velocities of 98, 131, 147, 155 and 164 m/s respectively for the 45%CO/15%H_2/40%N_2 mixture. These were chosen as they exhibit significant and varying degrees of extinction in the intermediate part of the flame and reignition further downstream as the local strain is relieved.

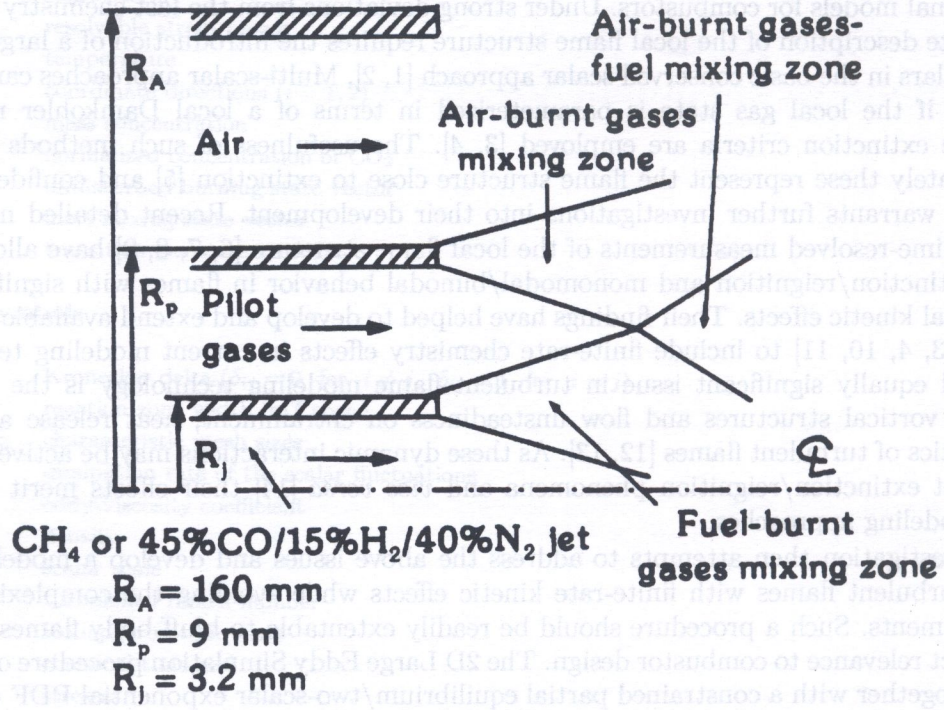

Fig. 1. Piloted diffusion flame burner geometry [8, 9]. (Pilot consists of either 45%CO/15%H_2/40%N_2 or CH_4 and air, fully burnt, depending on fuel tested)

3. Computational model formulation

3.1. Aerodynamic model

The aerodynamic model description derives from the formulation adopted in [13, 17]. Within the LES formalism the flow variables F can be decomposed in resolvable $\tilde{F}$, and subgrid scale F' quantities using a Favre-weighted filter, $\tilde{F} = \overline{\rho F}/\overline{\rho}$ ([18]). This results in the equations describing the resolvable flow quantities:

$$\frac{\partial \overline{\rho}}{\partial t} + \frac{\partial \overline{\rho}\tilde{u}}{\partial x_i} = 0 \qquad \frac{\partial \overline{\rho}\tilde{u}_i}{\partial t} + \frac{\partial(\overline{\rho}\tilde{u}_i\tilde{u}_j)}{\partial x_j} = -\frac{\partial \overline{p}}{\partial x_i} + \frac{\partial}{\partial x_j}\tilde{\sigma}_{ij} + \frac{\partial}{\partial x_j}\tau_{ij} + (\overline{\rho} - \rho_\infty)g_i \tag{1}$$

(ρ, μ, T and u represent density, viscosity, temperature and velocity of the gas and $i = 1, 2$ in a cartesian system (x, y)). $\overline{p} = \overline{\rho} R_u \tilde{T} \Sigma_i Y_i / M_i$ where Y_i, M_i are the mass concentration and molecular weight of specie i and R_u is the universal gas constant. $\tilde{\sigma}_{ij} = \mu(\tilde{S}_{ij} - 2/3\tilde{S}_{kk}\delta_{ij})$, τ_{ij} are the Sub-Grid Scale (SGS) stresses and $\tilde{S}_{ij}$ is the resolvable strain tensor. τ_{ij} is modeled as: $\tau_{ij} = -\overline{\rho u_i' u_j'} = \mu_{t,ij}(\tilde{S}_{ij} - (2/3)\tilde{S}_{kk}\delta_{ij}) - (2/3)\overline{\rho}\tilde{k}_s\delta_{ij}$, where $\tilde{k}_s$ is the subgrid kinetic energy obtained from a model equation of the form:

$$\frac{\partial \overline{\rho}\tilde{k}_s}{\partial t} + \frac{\partial(\overline{\rho}\tilde{u}_j\tilde{k}_s)}{\partial x_j} = \frac{\partial}{\partial x_j}\left[\left(\frac{\mu}{\sigma_k} + \frac{\mu_{tjj}}{\sigma_k}\right)\frac{\partial \tilde{k}_s}{\partial x_j}\right] - \overline{\rho u_i' u_j'}\frac{\partial \tilde{u}_i}{\partial x_j} - \frac{\mu_t}{\sigma_k}\frac{1}{\overline{\rho}^2}\frac{\partial \overline{\rho}}{\partial x_i}\frac{\partial \overline{p}}{\partial x_i}$$

$$-\frac{\rho_\infty}{\overline{\rho}^2}\frac{\mu_t}{\sigma_k}\frac{\partial \overline{\rho}}{\partial x_i}g_i - \overline{\rho}C_\varepsilon\frac{\tilde{k}^{3/2}}{L_t}(\sigma_k = 1.0) \tag{2}$$

The SGS eddy-viscosity could be evaluated from the SGS energy as: $\mu_t = \overline{\rho} C_k L_t \sqrt{\tilde{k}_s}$, with the SGS length scale given by $L_t = \Delta = \sqrt{\Delta x_i \Delta y_i}$ where Δ is the characteristic filter length (mesh size). As C_k has been reported to vary significantly in various simulations here we evaluated an anisotropic coefficient C_{kij} following the work of [19] who modeled the SGS fluctuations in proportion to the resolved stress tensor rather than the strain tensor. C_{kij} is obtained from the expression:

$$C_{kij} = \frac{(\overline{k}_s/\overline{k}_r)\overline{R}_{ij} + (2/3)\delta_{ij}\overline{k}_s}{\Delta\sqrt{\overline{k}_s}(2\overline{S}_{ij} - (2/3)\overline{S}_{kk}\delta_{ij})} \tag{3}$$

with the constraint $0.05 \leq C_{kij} \leq 0.5$. S_{ij}, R_{ij} and k_r are the resolved strain, stresses and fluctuating energy and $(-)$ denotes a statistical average. For a range of meshes and isothermal or reacting conditions this formulation proved quite satisfactory [13, 17].

3.2. Combustion model

3.2.1. Basic turbulence/chemistry interaction model

A simple partial equilibrium scheme was utilized by constraining the gas state with respect to a pre-specified CO_2concentration. This corresponds to a two-scalar description employing the mixture fraction, f, and the CO_2 concentration, Y_{CO_2}. The reaction CO + OH $\leftrightarrow$ CO_2 + H was employed to introduce non-equilibrium effects. CO_2 formation from CO is assumed to proceed primarily via this reaction at a rate: $\dot{r}_{CO_2} = k_f Y_{CO} Y_{OH} - (k_f/k_e) Y_{CO_2} Y_H$, with k_f taken as $6.76^{*}10^{11}\exp(T/1102)$ and k_e obtained from the JANAF tables. Whenever the mixture strength exceeds the rich flammability limit, the composition is diluted with fuel. Within this two-scalar description the final composition is calculated from the NASA equilibrium code for given f and Y_{CO_2} values by defining Y_{CO_2} as an 'element'. ρ, T, Y_i and $\dot{r}_{CO_2}$ values (the gas state vector $Y(f, Y_{CO_2})$) are obtained in a 2D library for $0 < f < 1$ and $0 < Y_{CO_2} < Y_{CO_{2,max}}$. The evolution of the passive, f, and the reactive, Y_{CO_2} variables, is calculated from the equations:

$$\frac{\partial(\overline{\rho}\tilde{f})}{\partial t} + \frac{\partial}{\partial x_j}(\overline{\rho}\tilde{u}_j\tilde{f}) = \frac{\partial}{\partial x_j}\left[\frac{\mu}{Sc}\frac{\partial \tilde{f}}{\partial x_j} - \overline{\rho u_j' f'}\right] \tag{4}$$

$$\frac{\partial(\overline{\rho}\tilde{Y}_{CO_2})}{\partial t} + \frac{\partial}{\partial x_j}(\overline{\rho}\tilde{u}_j\tilde{Y}_{CO_2}) = \frac{\partial}{\partial x_j}\left[\frac{\mu}{Sc}\frac{\partial \tilde{Y}_{CO_2}}{\partial x_j} - \overline{\rho u_j' Y_{CO_2}'}\right] + \overline{\rho}\tilde{\dot{r}}_{CO_2} \tag{5}$$

with $\overline{u_j' f'}$ and $\overline{u_j' Y_{CO_2}'}$ obtained with the help of the anisotropic SGS viscosity formulation as: $-\overline{\rho u_j' f'} = \frac{\mu_{tjj}}{Sc_t}\frac{\partial \tilde{f}}{\partial x_j}$, $-\overline{\rho u_j' Y_{CO_2}'} = \frac{\mu_{tjj}}{Sc_t}\frac{\partial \tilde{Y}_{CO_2}}{\partial x_j}$. An exponential joint PDF of the form $P(f^{*}, Y_{CO_2}^{*}) = \exp(a_1 + a_2 f^{*} + a_3 Y_{CO_2}^{*} + a_4 f^{*2} + a_5 Y_{CO_2}^{*2} + a_6 f^{*} Y_{CO_2}^{*})$ is constructed from the normalized mixture fraction and CO_2 concentration, f^{*} and $Y_{CO_2}^{*}$, which are used to transform the physical space of f and Y_{CO_2} into a normalized square area suitable for integration and is calculated parametrically through the coefficients $(a_1 - a_6)$ which depend on the local SGS moments $\overline{f'^2}$, $\overline{f_{CO_2}'^2}$, $\overline{f' Y_{CO_2}'}$. The SGS scalar fluctuation energy, $k_{fs} = 1/2\tilde{f}''^2$, is additionally obtained from the equation:

$$\frac{\partial(\overline{\rho}\tilde{k}_{fs})}{\partial t} + \frac{\partial(\overline{\rho}\tilde{u}_j\tilde{k}_{fs})}{\partial x_j} = \frac{\partial}{\partial x_j}\left[\left(\frac{\mu}{Sc} + \frac{\mu_{tjj}}{Sc_t}\right)\frac{\partial \tilde{k}_{fs}}{\partial x_j}\right] + (1/2)C_1\frac{\mu_t}{Sc_t}\frac{\partial \tilde{f}}{\partial x_j}\frac{\partial \tilde{f}}{\partial x_j} - \rho C_2 \frac{1}{\tau_t}\tilde{k}_{fs} \tag{6}$$

with $C_1 = C_2 = 2.0$ and $\tau_t = L_t/\sqrt{\tilde{k}_s}$. The remaining moments are modeled in line with the extended scale-similarity assumption used for the momentum field as follows: $\tilde{Y}_{CO_2}'^2 = (\overline{k}_{fs}/\overline{k}_{fr})R_{CO_2}$, $\overline{fY_{CO_2}} = (\overline{k}_{fs}/\overline{k}_{rs})R_{fCO_2}$, where $\overline{k}_{fr}$ is the resolved scalar fluctuation energy and R_{CO_2}, R_{fCO_2} are

the resolved fluctuations. The PDF constants are determined from normalization conditions and expressions for the moments resulting from integration of the PDF form. The mean gas state vector is evaluated by integration: $\tilde{Y} = (1/\overline{\rho}) \int Y \mathrm{J} \rho P(f^*, Y^*_{\mathrm{CO}_2}) df^* dY^*_{\mathrm{CO}_2}$, where J is the Jacobian of the transformation.

3.2.2. Extinction/reignition model

The modeling of finite-rate chemistry effects such as localized extinction and reignition derives from the analysis of [20]. Local extinction is predicted when the local Damkohler number,, $D\alpha_l$, defined as the ratio of the turbulent time scale, $\tau_\lambda = 3.88\tau_k$ (τ_k is the Kolmogorov time scale) to the chemical time scale, τ_{ch}, is below a local critical 'limit', $D\alpha_{cr}$ i.e.

$$\lambda = \frac{Da_1}{Da_{cr}} = \frac{[\tau_\lambda/\tau_{ch}]}{\left[\dfrac{\Sigma f}{\sqrt{2\Delta f_R}} \mathrm{Re}_t^{1/4}\right]} \leq 1 \tag{7}$$

Σ_f is the Gibson scale $\varepsilon_f^{1/2}(\nu/\varepsilon)^{1/4}$ where $\varepsilon, \varepsilon_f$ are the turbulence energy and scalar dissipation rates. Δf_R is the 'effective' reaction zone width in f space: $\Delta f_R = \Delta f_{RS} = f_R - f_L$ for $f_L \leq f \leq f_R$, $\Delta f_R = \Delta f_{RS} + f - f_R$ for $f > f_R$ and $\Delta f_R = \Delta f_{RS} + f_L - f$ for $f < f_L$. The chemical time scale may be taken from the partial equilibrium model as: $\tau_{ch} = 1/\dot{r}_{\mathrm{CO}_2}(f^*, Y^*_{\mathrm{CO}_2} = 0)$ for $f_L \leq f \leq f_R$, $\tau_{ch} = 1/\dot{r}_{\mathrm{CO}_2}(f^*_L, Y^*_{\mathrm{CO}_2} = 0)$ for $f < f_L$ and $\tau_{ch} = 1/\dot{r}_{\mathrm{CO}_2}(f^*_R, Y^*_{\mathrm{CO}_2} = 0)$ for $f > f_R$. The mean τ_{ch} value, determined by integration, is used in the criterion above.

Whenever Eq. (7) holds true extinction is predicted and the chemical source in Eq. (5) is set to zero. The post-extinction regime and the probable reignition behavior of the locally extinguished sample are modeled by the following gas states in f space: **a)** the $\mathbf{Y}_E = \mathbf{Y}_E(f^*, Y^*_{\mathrm{CO}_2})$ state representing undisturbed burning at partial equilibrium conditions when $\lambda > 1$. The mean gas state is determined as described in 3.2.1. **b)** the $\mathbf{Y}_O = \mathbf{Y}_O(f^*, Y^*_{\mathrm{CO}_2} \equiv 0)$ state representing the lower equilibrium bound and the Y_M limit state defined below. **c)** the $\mathbf{Y}_I = \mathbf{Y}_I(f^*)$ state representing inert mixing between fuel and air, and **d)** the intermediate state $\mathbf{Y}_Q$ between O and I, representing the gas state at the post-extinction transition phase from undisturbed burning to inert mixing and *vice versa*. $\mathbf{Y}_Q$ depends on $\tilde{f}$ and on the local values of the reactedness B : $B = (\mathbf{Y}_Q - \mathbf{Y}_I)/(\mathbf{Y}_O - \mathbf{Y}_I)$. The mean value $\tilde{Y}_Q$ can be obtained by convoluting with the local exponential PDF: $\tilde{Y}_Q = (1/\overline{\rho}) \int \int Y_Q \rho \mathrm{P}(\tilde{f}, \tilde{B}) df dB$. The required values of $\tilde{B}$ and B' are evaluated as described further below. Prior to this description reference to the analysis of [20] is required. It is demonstrated therein that the distributions of the time-average λ parameter with f (as determined from the data of [5, 6]) for various axial (CH_4) flame positions and fuel velocities close to extinction follow the curves shown in Fig. 2. When $\lambda < 1$ over the whole extent of the reaction zone width, Δf_{RS}, almost completely extinguished flame conditions result. It is further shown that the locally extinguished samples lie on a temperature curve which a) intersects the rich equilibrium branch at an f position coincident with the rich cross-over position of λ above 1 verifying the above criterion and b) the reactedness of this T distribution, EME′ (insert, Fig. 2) is well described by the equation $B_M = B_O \exp[-G(\lambda)^* \mathrm{Da_{cr}}]$. It should be remarked that this 'critical' Damkohler is a function of $\tilde{f}$ and f_{rms}. The above result is arrived at by using the IEM equations [16] to describe the particle evolution from the equilibrium to the mixing line: $dB/dt = (B_I - B)/\tau_e = -B/\tau_e$. Here τ_e is taken as $L_{R,t}/\sqrt{k_s}$, where $L_{R,t} = \dfrac{\sqrt{2}\Delta f_R}{\Sigma_t} \mathrm{Re}_t^{-3/4} * L_t$ is the reaction zone width in physical space ([5]) and it can be shown that: $\tau_e = \tau_\lambda/\mathrm{Da_{cr}}$. By integrating the IEM equation for the reactedness over an eddy turnover time, τ_λ, the M state (line EME') can be determined. The parameter $G = 1 - \lambda\gamma$ represents the effective decrease of the physical reaction zone width, $L_{R,t}$, in the transition phase from state O to I. $\gamma = (\Delta f_{RS}/f_S) - 1$ is a flame thickness parameter that addresses the effect of the reaction zone thickness in f space; $\gamma \approx 0$ for thin reaction zones (e.g. CH_4) denoting the more abrumpt reduction of $L_{R,t}$ in this case whilst $\gamma \approx 0.56$ for the $CO/H_2/N_2$ mixture. With

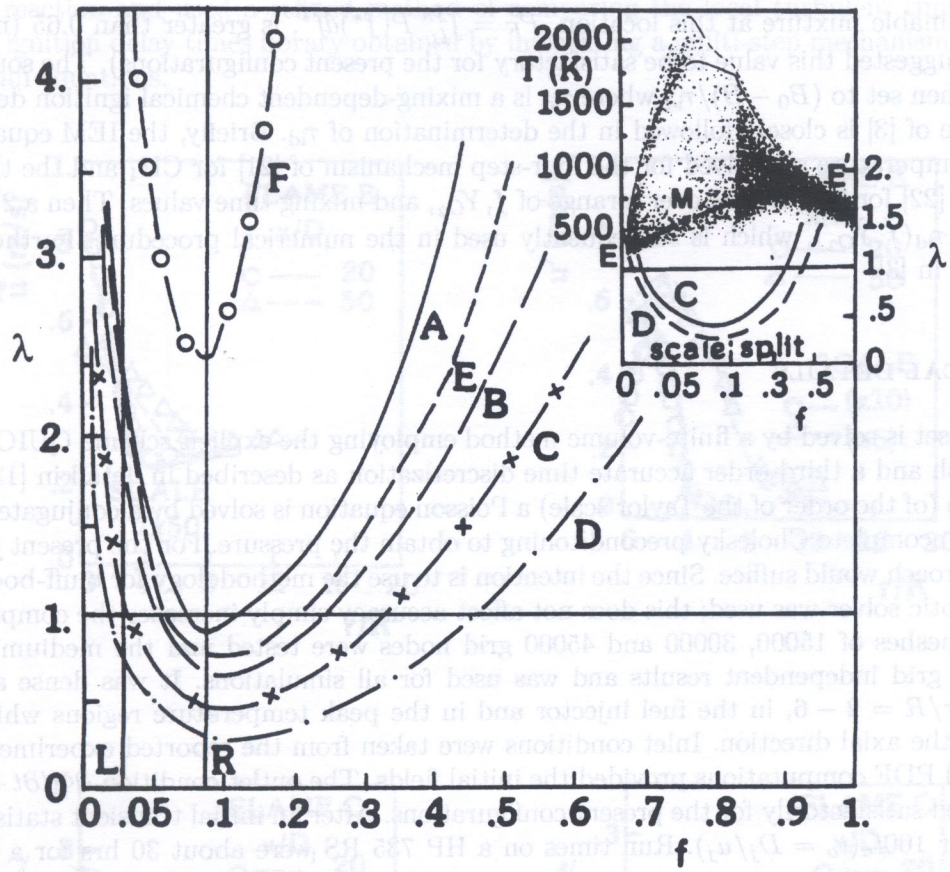

Fig. 2. Distributions of time-averaged λ values, eqn (7), for a range of CH_4 flame conditions (A: $u_j = 36$ m/s, $x/D_j = 20$, B: $u_j = 41$ m/s, $x/D_j = 20$, C: $u_j = 48$ m/s, $x/D_j = 20$, D: $u_j = 55$ m/s, $x/D_j = 20$, E: $u_j = 55$ m/s, $x/D_j = 30$, F: $u_j = 55$ m/s, $x/D_j = 50$, [5, 6]) -(insert) Comparison with the measured temperature scatterplot for flames C and D

these considerations in mind the resolved reactedness, $\tilde{B}$, is calculated from the following transport equation:

$$\frac{\partial(\rho\tilde{B})}{\partial t} + \frac{\partial(\overline{\rho}\tilde{u}_j\tilde{B})}{\partial x_j} = S_B \tag{8}$$

while its SGS fluctuations, $\tilde{B}'^2$ and $\overline{f}'\overline{B}'$ are obtained from the scale-similarity assumption. With the initial value of $\tilde{B}$ set by the partial equilibrium model the source term is maintained zero if no extinction has occurred and $S_B = (B_M - \tilde{B})/\tau_e$ after extinction has been detected. Equation (8) integrates in a Lagrangian sense the history of the state vector assuming that post-extinction mixing of the partial equilibrium products is represented by a deterministic relaxation to the inert value. The effect of the broadening of the reaction zone in f space e.g. due to dilution of fuel is accounted for and this is an aspect which has been stressed in a number of works ([5]) particularly in relation to the bimodal-monomodal behaviour close to extinction. According to the present formulation of Δf_R, the exchange time, τ_e, in the source of Eq. (8) for lean CH_4 compositions, which have a Δf_R of 0.055, is less than half the eddy time τ_λ. Integration over a time-step of the order of τ_λ will therefore produce either fully burned or extinguished states recovering the experimentally observed bimodal behavior of reactedness. For rich CH_4 compositions or in $CO/H_2/N_2$ mixtures Δf_R is almost ten times the above H/C values and τ_e attains values almost ten times those of lean CH_4 conditions. The above formulation then is expected to reproduce the gradual shift of measured scatterpoints to extinction for such fuels and compositions. Subsequent to extinction reignition is allowed when the time-scale criterion is inoperative and the cumulative propability of

finding a flammable mixture at this location, $P_F = \int_{f_L}^{f_R} P(f^*)df^*$, is greater than 0.65 (numerical experiments suggested this value to be satisfactory for the present configurations). The source term in Eq. (8) is then set to $(B_0 - \tilde{B})/\tau_{\rm id}$ where $\tau_{\rm id}$ is a mixing-dependent chemical ignition delay time. The procedure of [3] is closely followed in the determination of $\tau_{\rm id}$. Briefly, the IEM equations for species and temperature are solved for the four-step mechanism of [21] for CH_4 and the three-step mechanism of [22] for $CO/H_2/N_2$ over a range of f, Y_{O_2}, and mixing time values. Then a 2D library is built $\tau_{\rm id} = \tau_{\rm id}(\tilde{f}, \tilde{Y}_{O_2})$, which is subsequently used in the numerical procedure. Further details may be found in [3].

4. Numerical details

The equation set is solved by a finite-volume method employing the explicit scheme QUICKEST, a staggered mesh and a third-order accurate time discretization as described in detail in [13, 17]. At each time step (of the order of the Taylor scale) a Poisson equation is solved by a conjugate gradient method with incomplete Cholesky preconditoning to obtain the pressure. For the present jet flow a marching approach would suffice. Since the intention is to use the methodology for bluff-body flames as well an elliptic solver was used; this does not affect accuracy simply increases the computational time. Three meshes of 15000, 30000 and 45000 grid nodes were tested and the medium size was found to give grid independent results and was used for all simulations. It was dense along the shear layers, $r/R = 2 - 6$, in the fuel injector and in the peak temperature regions while it was expanding in the axial direction. Inlet conditions were taken from the reported experiments while $k-\varepsilon$/assumed PDF computations provided the initial fields. The outlet condition $\partial\Phi/\partial t + U_0(\partial\Phi/\partial x) = 0$ worked satisfactorily for the present configurations. After an initial transient statistics were computed over $100t_o(t_o = D_j/u_j)$. Run times on a HP 735 RS were about 30 hrs for a complete simulation.

5. Results and discussion

Statistical quantities and time-averaged data related to the development of the jet flames are presented and compared with the experimental data to appraise the model and identify its deficiencies. All figures are plotted with respect to the radial distance normalized by the fuel jet radius (Fig. 3). Comparisons are mostly made for axial stations, $x/D_j = 20, 30$ and 50 which are the most illustrative of the extinction/reignition phenomena occuring along the flame axis. Since experimental data for the mixing field have been reported only for the CH_4 flames [6] sample computations from these flames will be discussed first in brief to evaluate the performance of the aerodynamic model.

Figure 3 compares measured and calculated mean and *rms* axial velocities and mixture fraction for flames B and C. Mean and rms peak values near the axis and the low levels at about $r/R = 4$ have been reproduced well by the adopted LES/SGS model. Both near $(x/D_j = 20)$ and far field regions $(x/D = 30, 50)$ have also been calculated well. Discrepancies increase for flame C at the reignited region, $x/D_j = 50$, where an overprediction of about 15% is encountered near the centerline. Flame C with only a 7 m/s higher inlet jet velocity than flame B was found to mix slightly faster and this trend was faithfully followed in the computed fields.

Mixture fraction fluctuations compared quite favourably with data for both flames and stations with maximum disagreement of about 20% displayed for flame C. The scale-similarity assumption for the moments $\overline{f'^2}$, $\overline{f'Y_{CO_2}}$, $\overline{Y'^2_{CO_2}}$ apparently has worked satisfactorily. The present approach provided significantly improved predictions for the mixing field with respect to the results reported by [1] who employed a PDF transport method and a simple chemical model without kinetic effects. Present results are also somewhat better than the predictions of [11] obtained with a PDF transport model coupled to a second moment closure for the momentum field. The quality of the present simulations for the CH_4 results discussed so far, is similar to that reported in [3]. They considered

a global reaction and used a refined method of comparing the local turbulent time scale with a chemical ignition delay times library obtained by integrating a multi-step mechanism with the IEM Lagrangian equations.

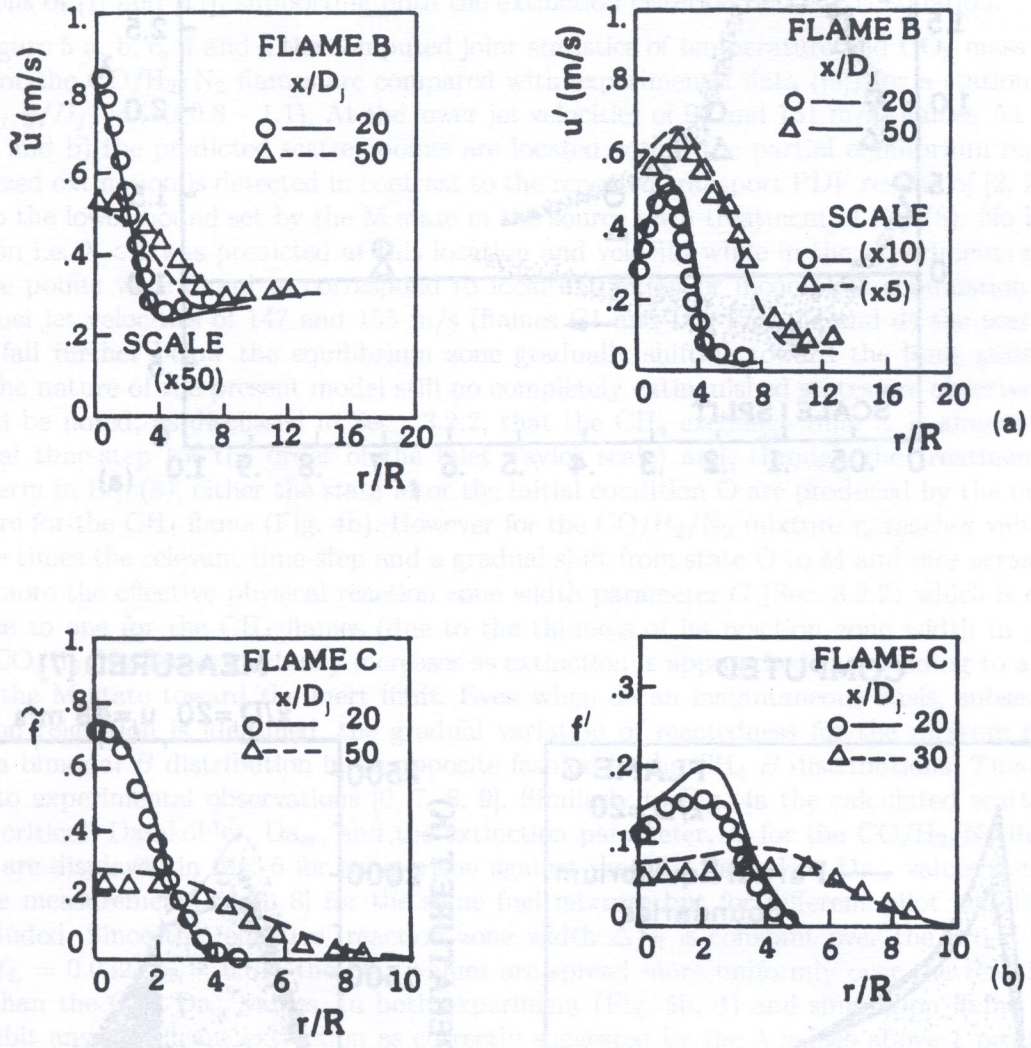

Fig. 3. Measured and calculated radial profiles for methane flames a) mean axial velocity and turbulence intensity (Flame B) and b) mean and RMS mixture fraction (Flame C).

Figure 4a displays the calculated scatterpoints for the 'critical' Damkohler, $\mathrm{Da_{cr}}$, and the extinction parameter, λ, plotted against mixture fraction for flame C ($x/D_j = 20$, $r/R = 1$ to 4). $\mathrm{Da_{cr}}$ values determined from the measurements [5] for flames B and C are also included. The $\mathrm{Da_{cr}}$ scatterpoints occupy an area that faithfully follows the experimentally deduced distributions corroborating the present extinction analysis (Fig. 2). As the local $\mathrm{Da_{cr}}$ is a function of $\tilde{f}$ and f_{rms} the flame positions with higher mixing rates will attain higher $\mathrm{Da_{cr}}$ distributions as illustrated in the displaced curves for flames B and C (Fig. 4a). Moreover their extinguished scatterpoints will fall to a lower M state limit (insert, Fig. 2), since $B_M = B_O \exp[-G(\lambda) * \mathrm{Da_{cr}}]$ in accord with experimental observation. Similarly the calculated λ values (Fig. 4a) for flame C cover well the experimentally determined distributions of Fig. 2 (curve C). In both analysis (Fig. 2) and simulation (Fig. 4a) λ is mostly below one accross the reaction zone width, Δf_{RS}, for flame C; according to Eq. (7) this location should be almost completely extingushed something verified in the discussion below.

Figure 4b presents the joint statistics between T and f for flame C together with experimental data for $x/D_j = 20$. The calculated plot shows that the predicted states mostly lie either on the

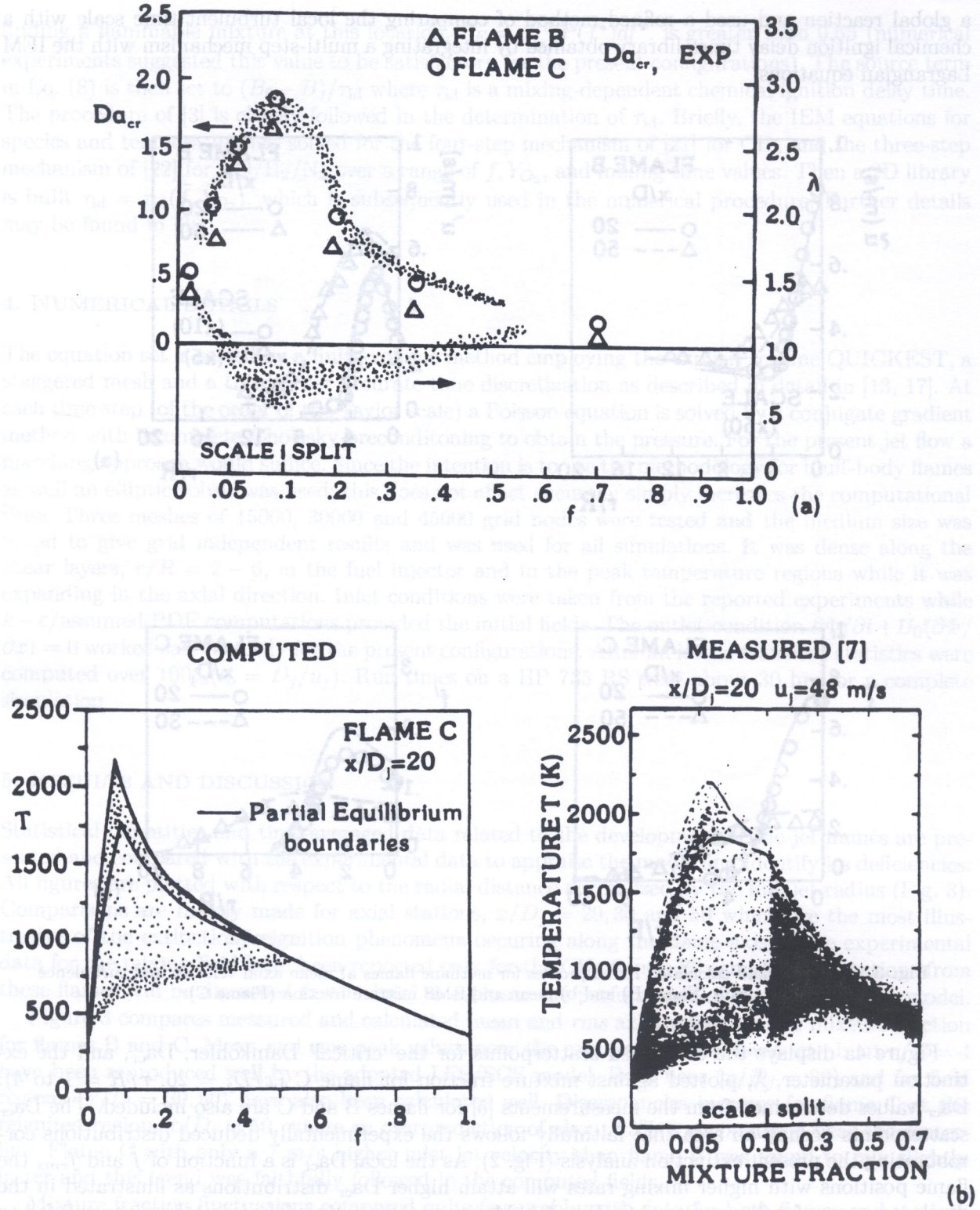

Fig. 4. a) Computed scatterplots of Da_{cr} and λ (Flame C, $x/D_j = 20$, $r/R_j = 1-4$). b) Joint PDF scatterplot in the T-f space (Flame C, $x/D_j = 20$, $r/R_j = 1-4$)

partial equilibrium zone or in the vicinity of the M state line with only a few points scattered in between. The model predicts bimodal pdfs with smaller variance than the experiment and with much less frequent intermediate points. Encouragingly the low temperature statistics have been reproduced along with the bimodal reactedness distributions and this is an improvement over the predictions of [1] and [11], supporting both the extinction criterion and the B equation.

In Figure 5 a, b, c, d and e the computed joint statistics of temperature and CO_2 mass fraction with f for the $CO/H_2/N_2$ flames are compared with experimental data ([9]) for a station located at $(x/D_j, y/D_j) = (10, 0.8 - 1.1)$. At the lower jet velocities of 98 and 131 m/s (flames A1 and B1, Figs. 5a and b) the predicted scatter points are located within the partial equilibrium region but no localized extinction is detected in contrast to the reported transport PDF results of [2, 22]. This is due to the lower bound set by the M state in the source term treatment of Eq. (8). No localized extinction i.e. $\lambda < 1$ was predicted at this location and velocity while in the experiments similarly only rare points were found to correspond to local extinction or incomplete combustion. At the higher fuel jet velocities of 147 and 155 m/s (flames C1 and D1, Figs. 5c and d) the scatterpoint profiles fall further below the equilibrium zone gradually shifting toward the limit state M but due to the nature of the present model still no completely extinguished states are observed. Again it should be noted, as discussed in Sec. 3.2.2, that the CH_4 exchange time τ_e is almost half the numerical time-step (of the order of the inlet Taylor scale) and, through the treatment of the source term in Eq. (8), either the state M or the initial condition O are produced by the numerical procedure for the CH_4 flame (Fig. 4b). However for the $CO/H_2/N_2$ mixture τ_e reaches values more than five times the relevant time-step and a gradual shift from state O to M and *vice versa* results. Furthermore the effective physical reaction zone width parameter G (Sec. 3.2.2) which is constant and close to one for the CH_4 flames (due to the thinness of its reaction zone width in f space) for the $CO/H_2/N_2$ flames gradually increases as extinction is approached thus leading to a gradual shift of the M state toward the inert limit. Even when on an instantaneous basis, subsequent to extinction reignition is identified, the gradual variation of reactedness for the mixture does not lead to a bimodal B distribution in an opposite fashion to the CH_4 B distributions. This trend is similar to experimental observations [6, 7, 8, 9]. Similarly to Fig. 4a the calculated scatterpoints for the 'critical' Damkohler, Da_{cr}, and the extinction parameter, λ, for the $CO/H_2/N_2$ flames B1 and D1 are displayed in Fig. 6 for comparison against the CH_4 data. Few Da_{cr} values determined from the measurements of [5, 8] for the same fuel mixture but for different pilot conditions are also included. Since the 'effective' reaction zone width Δf_R is constant over the broad reaction limits ($f_L = 0.032, f_R = 0.61$) the Da_{cr} values are spread more uniformly over the reaction zone extent than the CH_4 Da_{cr} values. In both experiment (Fig. 5b, d) and simulation flame B1 does not exhibit any significant extinction as correctly suggested by the λ values above 1 produced by the present extinction treatment; in contrast flame D1 suffers quite significant local extinctions and produces much lower λ values. A shortcoming of the present partial equilibrium scheme [10] was made evident in the $CO/H_2/N_2$ calculations in the prediction of species such as H_2O and H_2. Since Y_{H_2} is overpredicted by about a factor of 1.7 the initial partial equilibrium condition would be in error in the extinction treatment. A remedy could be either to use the chemical scheme of [12] or to exploit a flamelet library [12] and relate its strain parameter to $\dot{r}_{CO_2}$ retaining the present equation system. Finally at $u_j = 164$ m/s (flame E1, Fig. 5e) most of the predicted state locations are toward the unreacted limit with only a small amount of states found in the transition phase between the lower equilibrium bound ($\mathbf{Y}_O(f^*, Y^*_{CO_2} \equiv 0)$) and the M state suggesting a rapid decrease in the probability of reignition. The conditional averages for the three velocities were in rather good agreement with measurements for both temperature and Y_{CO_2} with a maximum discrepancy of about $17 - 23\%$ for the higher jet velocity. Global extinction of the $CO/H_2/N_2$ flame configuration was computed at a jet velocity of 180 m/s while the experimental blow-off velocity was 167 m/s. The proposed B equation resembles in a way the coalescence/dispersion model in Monte-Carlo/PDF calculations (e.g. [11]). When used together with the extinction criterio it takes into account through the formulated exchange time, τ_e, the effects of combustion on mixing and is effective at large or small Damkohler numbers. It is recognised of course that, as in the coalescence/dispersion model,

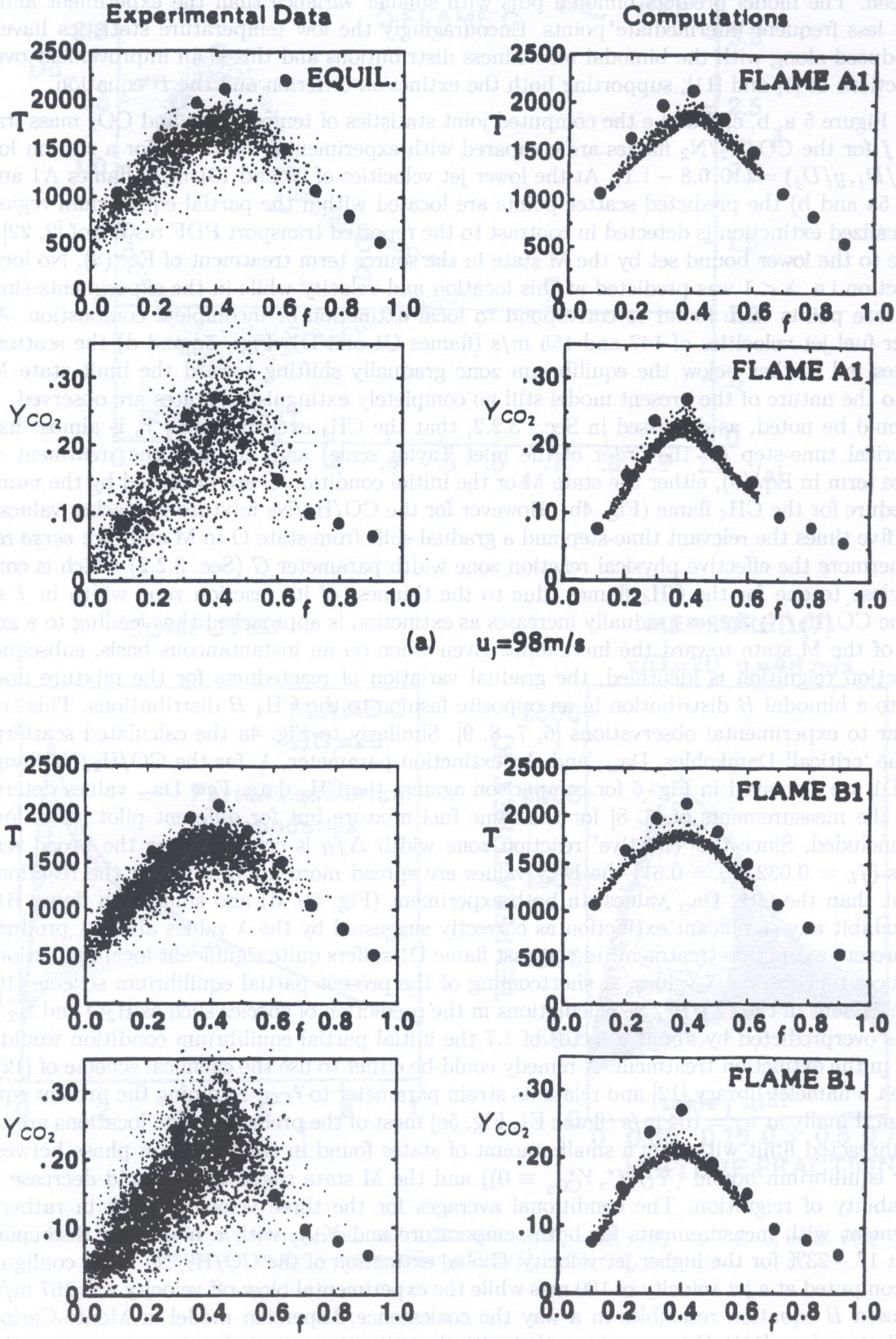
Experimental Data
Computations
EQUIL.
FLAME A1
FLAME A1
T
Y_{CO_2}
f
(a) u_j=98m/s
FLAME B1
FLAME B1
(b) u_j=131m/s

[Fig. 5a,b]

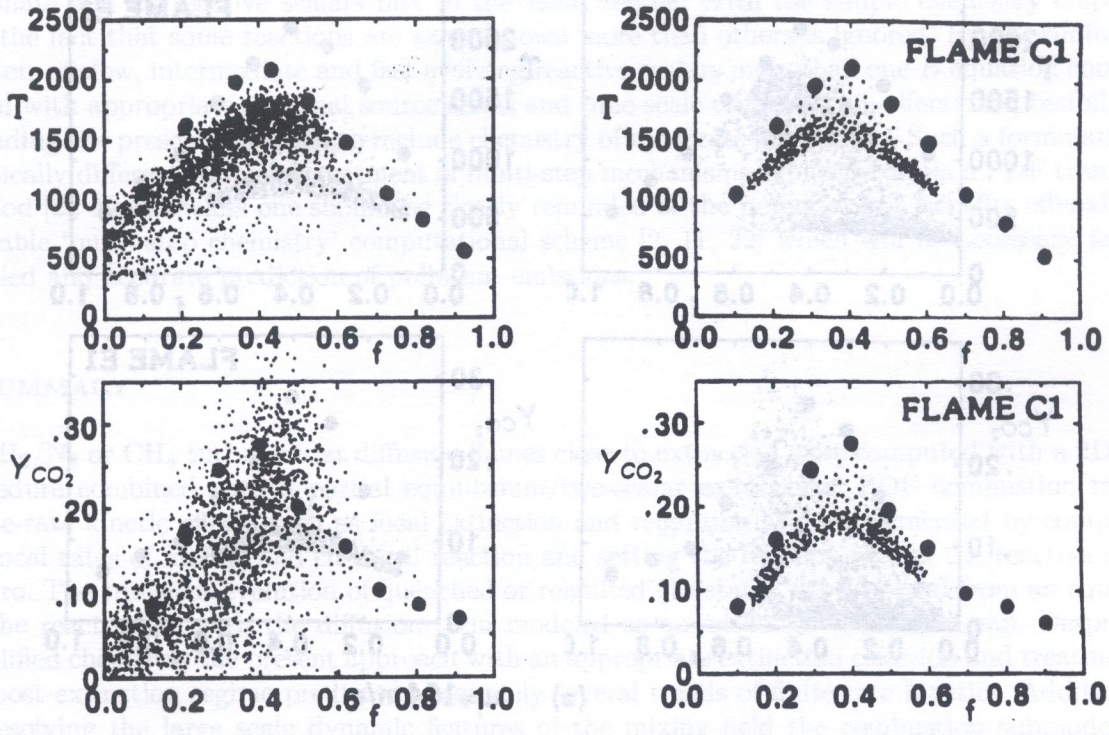

(c) u_j=147m/s

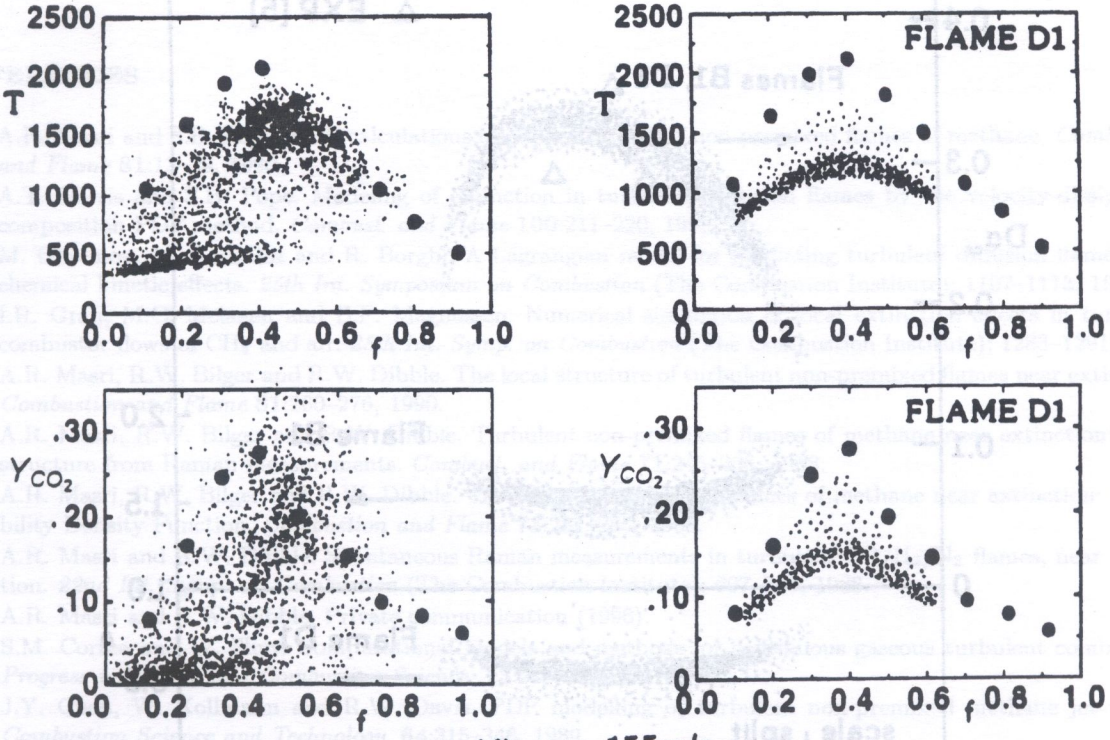

(d) u_j=155m/s

[Fig. 5c,d]

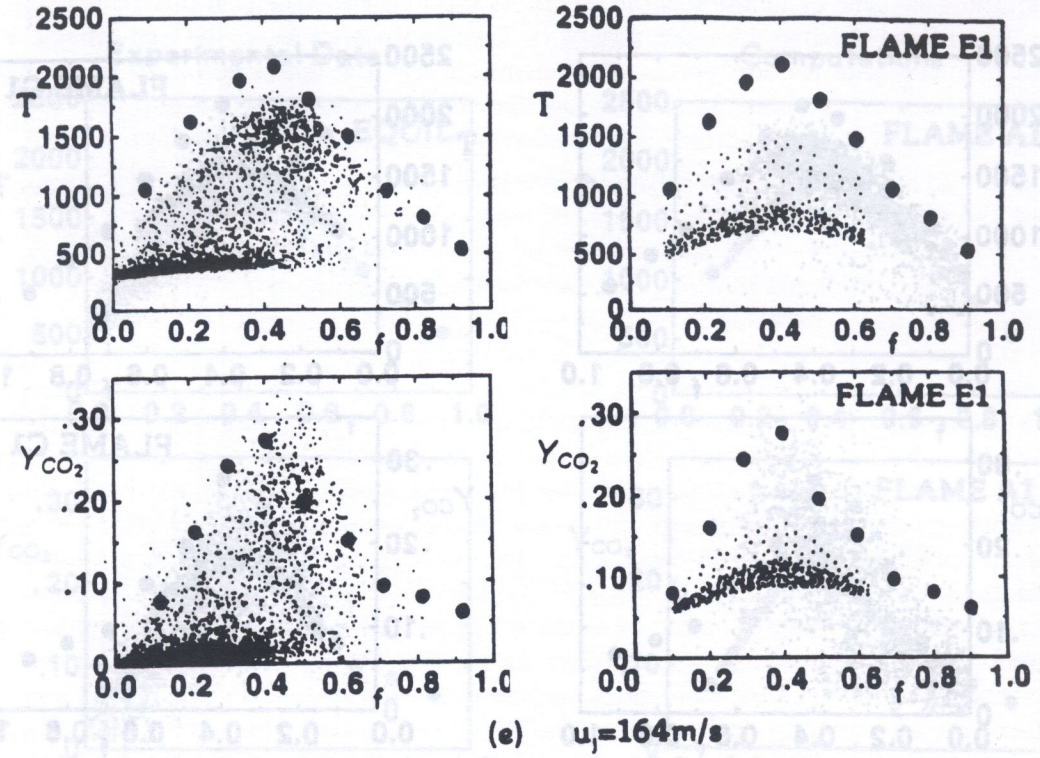

Fig. 5. Measured and computed composition scatterplots for the $CO/H_2/N_2$-air flames, experimental data of [8, 9]

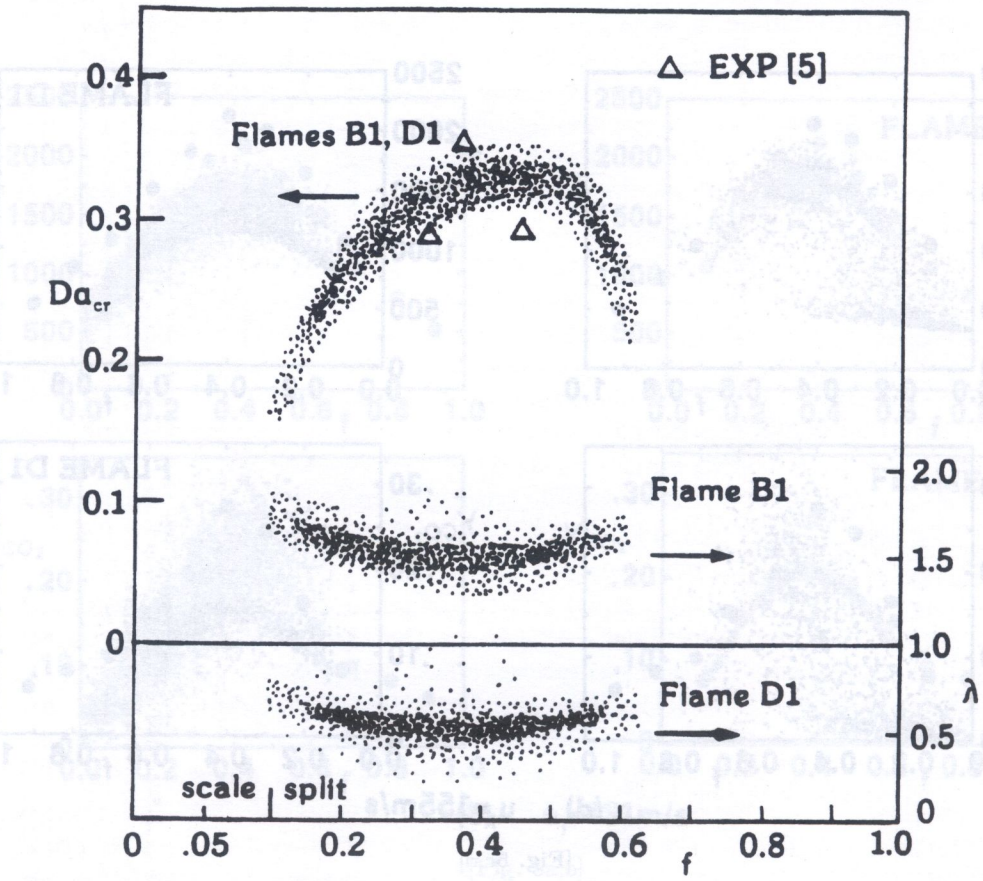

Fig. 6. Computed scatterplots of D and (Flames B1 and D1, $x/D_j = 10$, $r/R_j = 0.8 - 1.1$)

implicit in the use of the B equation is the assumption that once extinction is detected all reactions terminate and all reactive scalars mix to the same degree. With the simple chemistry employed here the fact that some reactions are slowed down more than others is ignored. By discriminating into sets of slow, intermediate and fast evolving reactive scalars more than one B equation could be solved with appropriate chemical source terms and time-scale criteria. This offers one possibility of extending the present approach to include chemistry of moderate complexity. Such a formulation is drastically different from the treatment of multi-step mechanisms explicitly or via a PDF transport method [2]. Nevertheless one should be clearly reminded of the potential and benefits offered by a tractable 'multi-step chemistry' computational scheme [2, 11, 22] which will be necessary for the detailed and accurate prediction of pollutant emissions.

6. SUMMARY

$CO/H_2/N_2$ or CH_4 turbulent jet diffusion flames close to extinction were computed with a 2D LES procedure combined with a partial equilibrium/two-scalar exponential PDF combustion model. Finite-rate kinetic effects such as local extinction and reignition were implemented by comparing the local rates of mixing and chemical reaction and setting the reaction rate of the reactive scalar to zero. The transient evolution of quenched or reignited gas states was obtained from an equation for the reactedness with the diffusion term modeled as an exchange with the mean. Despite its simplified chemistry the present approach with an appropriate extinction criterion and treatment of the post-extinction regime predicted adequately several trends of finite-rate kinetics. Additionally by resolving the large scale dynamic features of the mixing field the combustion submodel was exploited effectively while the assumption of a PDF shape seemed less critical at the small scale level. The method, through further tests and refinements, could be useful for the calculation of burner stability, the study of flows with active control of combustion or the calculation of bluff-body flames.

REFERENCES

[1] A.R. Masri and S.B. Pope. PDF calculations of piloted turbulent non-premixed flames of methane. *Combustion and Flame* **81**:13–29, 1990.

[2] A.T. Norris and S.B. Pope. Modeling of extinction in turbulent diffusion flames by the velocity-dissipation-composition PDF method. *Combust. and Flame* **100**:211–220, 1995.

[3] M. Obounou, M. Gonzalez and R. Borghi. A Lagrangian model for predicting turbulent diffusion flames with chemical kinetic effects. *25th Int. Symposium on Combustion* (The Combustion Institute); 1107–1113, 1994.

[4] I.R. Gran, M.C. Melaaen and B.F. Magnussen. Numerical simulation of local extinction effects in turbulent combustor flows of CH_4 and air. *25th Int. Symp. on Combustion* (The Combustion Institute); 1283–1291, 1994.

[5] A.R. Masri, R.W. Bilger and R.W. Dibble. The local structure of turbulent non-premixed flames near extinction. *Combustion and Flame* **81**:260–276, 1990.

[6] A.R. Masri, R.W. Bilger and R.W. Dibble. Turbulent non-premixed flames of methane near extinction: Mean structure from Raman measurements. *Combust. and Flame* **71**:245–266, 1988.

[7] A.R. Masri, R.W. Bilger and R.W. Dibble. Turbulent non-premixed flames of methane near extinction: Propability Density Function. *Combustion and Flame* **73**:261–285, 1988.

[8] A.R. Masri and R.W. Dibble. Spontaneous Raman measurements in turbulent $CO/H_2/N_2$ flames, near extinction. *22nd Int. Symp. on Combustion* (The Combustion Institute); 607–618, 1988.

[9] A.R. Masri and R.W. Dibble. Private communication (1996).

[10] S.M. Correa and W. Shyy. Computational models and methods for continuous gaseous turbulent combustion. *Progress in Energy and Combustion Science*, **13**:249–292, 1987.

[11] J.Y. Chen, W. Kollmann and R.W. Davis. PDF modelling of turbulent non-premixed methane jet flames. *Combustion Science and Technology*, **64**:315–346, 1989.

[12] F. Fichot, B. Delhaye, D. Veynante and S.M. Candel. Strain rate modeling for a flame surface density equation with application to non-premixed turbulent combustion. *25th Int. Symp. on Combustion* (The Combustion Institute); 1273–1281, 1994.

[13] P. Koutmos, C. Mavridis and D. Papailiou. A study of turbulent diffusion flames formed by planar fuel injection into the wake formation region of a slender square cylinder. *26th Int. Symp. on Combustion* (The Combustion Institute); 161–168, 1996.

[14] F. Takahashi, W.J. Schmoll, D.D. Trump and L.P. Goss. Vortex-flame interactions and extinction in turbulent jet diffusion flames. *26th Int. Symp. on Combustion* (The Combustion Institute); 145–152, 1996.

[15] T.S. Cheng and R.W. Pitz. Simultaneous measurement of conserved and reactive scalars in turbulent diffusion flames for assessment of PDF models. *25th Int. Symposium on Combustion* (The Combustion Institute); 1133–1139, 1994.

[16] R. Borghi, Turbulent combustion modelling. *Progress in Energy and Combustion Science*, **14**:245–292, 1988.

[17] P. Koutmos, C. Mavridis and D. Papailiou. A study of unsteady wake flows past a two- dimensional square cylinder with and without planar jet injection into the vortex formation region. *Applied Scientific Research* **55**:187–210, 1996.

[18] S. Menon and W.H. Calhoon. Subgrid mixing and molecular transport modeling in a reacting shear layer. *26th Int. Symp. on Combustion* (The Combustion Institute); 59–66, 1996.

[19] T. Goutorbe, D. Laurence and V. Maupu. An apriori test of an SGS tensor model including anisotropy and backscatter effects in Direct and Large Eddy Simulations I. Voke *et al.* eds., Kluwer Academic Publishers, 1994.

[20] P. Koutmos. A Damkohler number description of local extinction in CH_4 jet diffusion flames. *FUEL*, 78(5), 623–626, 1999.

[21] R.W. Bilger, S.H. Starner and R.J. Kee. On reduced mechanism for CH4-air combustion in non-premixed flames. *Combust. Flame*, **80**:135–150, 1990.

[22] J.Y. Chen, R.W. Dibble and R.W. Bilger. Modeling of turbulent non-premixed $CO/H_2/N_2$ jet flames with reduced mechanism. *23rd Int. Symp. on Combustion* (The Combustion Institute); 775–780, 1990.